



**Please cite the Published Version**

Peng, Ting, Wu, Ruiqing, Wang, Bohai, Liskiewicz, Tomasz  and Shi, Shengwei  (2024) Long-Term Storage of Ti<sub>3</sub>C<sub>2</sub>T<sub>x</sub> Aqueous Dispersion with Stable Electrochemical Properties. *Materials*, 17 (22). 5414 ISSN 1996-1944

**DOI:** <https://doi.org/10.3390/ma17225414>

**Publisher:** MDPI AG

**Version:** Published Version

**Downloaded from:** <https://e-space.mmu.ac.uk/637102/>

**Usage rights:**  [Creative Commons: Attribution 4.0](https://creativecommons.org/licenses/by/4.0/)


**Additional Information:** This is an open access article which first appeared in *Materials*, published by MDPI

**Enquiries:**

If you have questions about this document, contact [openresearch@mmu.ac.uk](mailto:openresearch@mmu.ac.uk). Please include the URL of the record in e-space. If you believe that your, or a third party's rights have been compromised through this document please see our Take Down policy (available from <https://www.mmu.ac.uk/library/using-the-library/policies-and-guidelines>)

Article

# Long-Term Storage of $Ti_3C_2T_x$ Aqueous Dispersion with Stable Electrochemical Properties

Ting Peng <sup>1,2,†</sup>, Ruiqing Wu <sup>1,†</sup>, Bohai Wang <sup>1</sup>, Tomasz Liskiewicz <sup>3,\*</sup>  and Shengwei Shi <sup>1,4,\*</sup> 

<sup>1</sup> Hubei Key Laboratory of Plasma Chemistry and Advanced Materials, School of Materials Science and Engineering, Wuhan Institute of Technology, Wuhan 430205, China; pt@xjtu.edu.cn (T.P.); 22305010031@stu.wit.edu.cn (R.W.); 22205010032@stu.wit.edu.cn (B.W.)

<sup>2</sup> School of Chemical and Environmental Engineering, Xinjiang Institute of Engineering, Urumqi 830002, China

<sup>3</sup> Faculty of Science and Engineering, Manchester Metropolitan University, Manchester M15 6BH, UK

<sup>4</sup> Key Laboratory of Optoelectronic Chemical Materials and Devices (Ministry of Education), Jiangnan University, Wuhan 430056, China

\* Correspondence: t.liskiewicz@mmu.ac.uk (T.L.); shisw@wit.edu.cn (S.S.)

† These authors contributed equally to this work.

**Abstract:** MXenes possess high metallic conductivity and excellent dispersion quality and pseudocapacitance. Their good hydrophilicity makes them particularly suitable as eco-friendly inks for printing applications. However, MXenes are prone to oxidation in aqueous dispersions, and it is very important to improve their stability. Here, the long-term storage of MXene aqueous dispersions was realized by the introduction of sodium L-ascorbate (NaAsc) as the antioxidant. The preserved MXenes exhibited very stable electrochemical properties. Even after 60-day storage, the supercapacitor with preserved MXenes as the electrode still demonstrated an excellent specific capacitance of 381.1 F/g at a scan rate of 5 mV/s and a good retention rate of 92.6% after 10,000 consecutive cyclic voltammetry measurements, which was nearly the same as that of fresh MXenes. The results indicate a facile and efficient method to realize the long-term storage of MXene aqueous dispersions for mass use in future energy storage.

**Keywords:** MXene; stability; long-term storage; sodium L-ascorbate; supercapacitor



**Citation:** Peng, T.; Wu, R.; Wang, B.; Liskiewicz, T.; Shi, S. Long-Term Storage of  $Ti_3C_2T_x$  Aqueous Dispersion with Stable Electrochemical Properties. *Materials* **2024**, *17*, 5414. <https://doi.org/10.3390/ma17225414>

Academic Editor: Valery N. Khabashesku

Received: 12 September 2024

Revised: 22 October 2024

Accepted: 25 October 2024

Published: 6 November 2024



**Copyright:** © 2024 by the authors. Licensee MDPI, Basel, Switzerland. This article is an open access article distributed under the terms and conditions of the Creative Commons Attribution (CC BY) license (<https://creativecommons.org/licenses/by/4.0/>).

## 1. Introduction

MXene is a two-dimensional (2D) layered carbide/nitride, generally denoted by the chemical formula of  $M_{n+1}X_nT_x$ , where M represents the early transition metal element, X stands for C/N, and T is the surface group (such as -OH, -F, -Cl, etc.) [1]. The diverse and tunable surface chemistry of MXene affords it valuable and distinctive properties [2,3]. For example, the etching of the MAX phase with HF or LiF/HCl results in an MXene with -F groups on the external surface [4,5], while the alkali treatment can be applied to prepare MXenes without -F groups [6]. In addition, surface functional groups can be regulated by annealing at high temperatures [7]. Due to their distinctive structure and excellent properties, MXenes have been broadly applied in different fields such as sensors [8–12], supercapacitors [13–18], metal-ion batteries [19–22], photo/electrocatalysis [23–26], electromagnetic interference shielding [27–32], optoelectronics [33–37], and others [38–41].

However, MXene is prone to degrade, especially in aqueous dispersions [42,43]. The key factor for the instability of MXene was considered to be oxidation in the presence of water, and the dissolved oxygen in water was found to be fatal to MXenes in aqueous dispersions [44]. A cost-effective and eco-friendly way for long-term storage of MXenes in aqueous solution was reported based on the hydration chemistry of nontoxic inorganic salts [42], in which the attacking of MXene by dissolved oxygen molecules was restricted by reducing the water activity, as the concentration of dissolved oxygen greatly decreased in a NaCl solution. To reduce the oxidation of MXenes, various methods have been applied.

Preparing different MAX phases is a feasible way to improve the stability of MXene due to different structures and surface groups in obtained MXenes [45,46]. Refrigerated cryogenic storage also can effectively prolong MXene stability in water at high cost [47–49]. As the storage of MXenes in organic solvents can provide an environment with low oxygen content, the stability of MXenes can be obviously enhanced [50–52]. The passivation of the MXene surface via the deep eutectic solvents method can extend its lifetime to 28 weeks, which is effective not only for MXene in a solution but also for that in a dry state [53]. In addition, high temperature annealing can induce a structure change in MXenes, and remove the inherent water molecules; thus, the stability of the MXene aqueous dispersion is effectively prolonged [54,55]. Furthermore, since the oxidization starts from the edge defects, MXene edges have been generally modified by anionic groups such as polyphosphates, polyborates, or polysilicates, which allows MXenes to be stored for more than three weeks [56]. The storage of MXenes with citric acid can improve MXene stability up to 5 months, but a large amount of citric acid is required [57]. Although sodium L-ascorbate (NaAsc) has been reported to effectively preserve  $Ti_3C_2T_x$  MXenes for up to 21 days [58], there has not been enough investigation centered on a longer period of time, and the effect on the electrochemical property of MXenes has not been investigated.

Here, the long-term storage of MXene aqueous dispersions with NaAsc as the antioxidant was investigated mainly based on the consideration of electrochemical properties. The passivation of NaAsc to MXene nanosheet defects/edges protected the MXene from the reaction with dissolved oxygen in water. In addition, the strong interaction between NaAsc and water reduced the content of dissolved oxygen in the water. MXenes can be well stored for 60 days in the atmosphere without any degradation of their electrochemical properties. The specific capacitance still reaches 381.1 F/g at a scan rate of 5 mV/s after 60 days of storage with NaAsc, and the retention rate is 92.6%. The results indicated a low-cost, facile, and effective way to store MXene aqueous dispersions as well as great potential as eco-friendly inks for printing processes in the future. Thus, our findings propose an effective approach for the long-term storage of MXene with minimal attenuation of its electrochemical performance.

## 2. Experimental Section

### 2.1. Materials

$Ti_3AlC_2$  was purchased from Foshan Xinene Technology Co., Ltd. (Foshan, China). Lithium Fluoride (LiF, 99%) and Tetramethylammonium Hydroxide (TMAOH, 25%) were obtained from Shanghai Macklin Biochemical Technology Co., Ltd. (Shanghai, China). Hydrochloric acid (HCl, AR) was purchased from Sinopharm Chemical Reagent Co., Ltd. (Shanghai, China). Ethanol absolute (EtOH, AR) was obtained from Hubei Forton Science and Technology Co., Ltd. (Wuhan, China). NaAsc was bought from Shanghai Aladdin Reagent Co., Ltd. (Shanghai, China).

### 2.2. Preparation of MXenes

Take 3 g of LiF and  $Ti_3AlC_2$  each, prepare 60 mL HCl (9 mol/L), add the prepared HCl to the three-necked flask, slowly add LiF to the three-necked flask, and stir with a constant-temperature magnetic stirrer for 10 min until LiF is completely dissolved in HCl; slowly add 3 g of  $Ti_3AlC_2$  to the three-necked flask in the above step using an ice bath, and then place in an oil bath at 40 °C for continuous stirring for 48 h. After the reaction is completed, centrifuge the reactant at 10,000 rpm for 10 min, remove the supernatant, and add deionized water (DI water) to the centrifuge tube, centrifuge at speed for 10 min, and repeat the centrifugation 5–6 times until the pH of the supernatant is close to 6; remove the lower layer of precipitate and add 20 mL of TMAOH by hand to make it dispersed evenly, and stir the intercalation layer with a constant-temperature magnetic stirrer for 5 h. Divide the MXene aqueous dispersion after TMAOH intercalation into three centrifuge tubes, add EtOH and centrifuge twice at 10,000 rpm for 10 min each time, and then add DI water and centrifuge twice at 10,000 rpm for 10 min each time. After centrifugation,

remove the supernatant, collect the lower precipitate, add DI water and shake it to make it evenly dispersed, ultrasonicate for 1 h, and finally centrifuge at 4000 rpm for 35 min. The dark green supernatant liquid is taken as a few-layer dispersion liquid (high-concentration  $\text{Ti}_3\text{C}_2\text{T}_x$  dispersion), and the product  $\text{Ti}_3\text{C}_2\text{T}_x$  powder can be obtained by vacuum filtration and drying of the dispersion liquid.

### 2.3. Preparation of MXene-NaAsc Aqueous Dispersion

To 50 mg of  $\text{Ti}_3\text{C}_2\text{T}_x$  powder, add 50 mL of DI water to ultrasonicate for 30 min, and prepare a uniformly dispersed 1 mg/mL  $\text{Ti}_3\text{C}_2\text{T}_x$  aqueous dispersion. Weigh 50 mg of NaAsc powder, add it to the  $\text{Ti}_3\text{C}_2\text{T}_x$  aqueous dispersion, and sonicate for 30 min to obtain a uniform 50 mL 1 mg/mL  $\text{Ti}_3\text{C}_2\text{T}_x$ -NaAsc aqueous dispersion. To preserve the stability of the dispersion, the concentration of NaAsc must be consistently maintained at 1 mg/mL [58]. Then, transfer the NaAsc-MXene dispersion and the fresh MXene aqueous dispersion to transparent glass vials, and place them in a room temperature environment without any manual manipulation for future use.

$\text{Ti}_3\text{C}_2\text{T}_x$  aqueous dispersion for different storage times was represented as  $\text{Ti}_3\text{C}_2\text{T}_x$ - $\text{H}_2\text{O}$ -x or  $\text{Ti}_3\text{C}_2\text{T}_x$ -NaAsc-x, in which x indicated the number of days.

### 2.4. Characterizations

Vacuum filter the freshly prepared  $\text{Ti}_3\text{C}_2\text{T}_x$  aqueous dispersion ( $\text{Ti}_3\text{C}_2\text{T}_x$ -Fresh) and the  $\text{Ti}_3\text{C}_2\text{T}_x$  aqueous dispersion stored with NaAsc for 15 days ( $\text{Ti}_3\text{C}_2\text{T}_x$ -NaAsc-15) and 30 days ( $\text{Ti}_3\text{C}_2\text{T}_x$ -NaAsc-30) to obtain their powders for further characterizations. Conduct X-ray diffraction (XRD, Germany) to obtain the crystalline structure with a D8 ADVANCE X-ray diffractometer. Measure UV-vis spectra with Lambda 35 UV spectrophotometer. Characterize the morphology using a JSM-5510LV scanning electron microscope (SEM, Tokyo, Japan) and JEM2100 transmission electron microscopy (TEM, Tokyo, Japan), and analyze the detailed elements by X-ray photoelectron spectroscopy (XPS, UK) with ESCALAB Xi+ X-ray photoelectron spectrometer.

### 2.5. Electrochemical Measurement

Preparation of electrodes: Grind 24 mg of  $\text{Ti}_3\text{C}_2\text{T}_x$  sample into powder, and then mix it with activated carbon and polytetrafluoroethylene (PTFE) in a mass ratio of 8:1:1; add a drop of N-methylpyrrolidone (NMP) to make it fully ground, and spread it evenly on  $1 \times 1.5 \text{ cm}^2$  foam copper substrate, under the pressure of 10 MPa. Press the weighed working electrode on a tablet press for 1 min, and then put it into a vacuum drying oven to dry to constant weight. Soak the prepared electrode in 1 mol/L  $\text{H}_2\text{SO}_4$  electrolyte for 12 h to ensure that the electrolyte can fully penetrate the electrode material.

Electrochemical measurements: All electrochemical measurements were performed by a CHI660E electrochemical workstation (Shanghai Chenhua Instrument Co., Ltd., Shanghai, China). Three-electrode configuration was applied for electrochemical measurements, with  $\text{Ti}_3\text{C}_2\text{T}_x$  as the working electrode, Ag/AgCl as the reference electrode, activated carbon as the counter electrode, and 1 mol/L  $\text{H}_2\text{SO}_4$  as the electrolyte. Cyclic voltammetry (CV) at different scan rates of 5–200 mV/s, galvanostatic charge/discharge (GCD) at 1–5 A/g, and CV cycling tests at 50 mV/s scan rate were measured. The volumetric capacitance is determined from the CV data by using the following equation:

$$C = \frac{1}{\Delta V} \int \frac{idV}{v} \quad (1)$$

where C is the normalized capacitance, i is the current density, v is the voltage scan rate, V is the voltage, and  $\Delta V$  is the voltage window.

## 3. Results and Discussion

Figure 1 shows the preparation of the  $\text{Ti}_3\text{C}_2\text{T}_x$  aqueous dispersion by ultrasonic treatment. The fresh  $\text{Ti}_3\text{C}_2\text{T}_x$  aqueous dispersion was black whether NaAsc was added or not.

$\text{Ti}_3\text{C}_2\text{T}_x\text{-H}_2\text{O}$  showed poor stability due to the self-stacking of the MXene in the aqueous dispersion. After 30-day storage in the atmosphere, a large amount of precipitations were found in  $\text{Ti}_3\text{C}_2\text{T}_x\text{-H}_2\text{O-30}$ , resulting in the color change to faint black, while there was no precipitation in  $\text{Ti}_3\text{C}_2\text{T}_x\text{-NaAsc-30}$ , and it remained a black and uniform dispersion after 30 days, indicating the improved stability of  $\text{Ti}_3\text{C}_2\text{T}_x$ , which may result from the restricted self-stacking of  $\text{Ti}_3\text{C}_2\text{T}_x$  with the introduction of NaAsc.

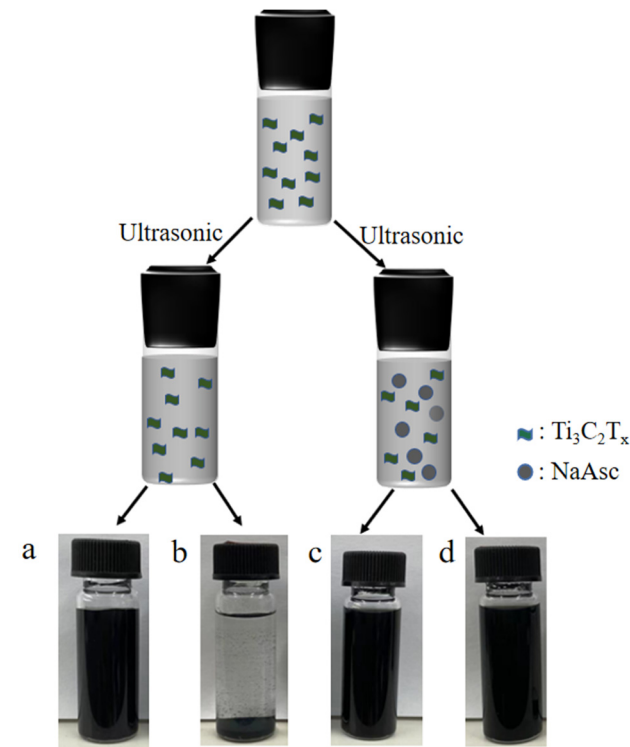


**Figure 1.** Photographs of  $\text{Ti}_3\text{C}_2\text{T}_x$  aqueous dispersions by ultrasonic treatment. (a)  $\text{Ti}_3\text{C}_2\text{T}_x\text{-H}_2\text{O-0}$ ; (b)  $\text{Ti}_3\text{C}_2\text{T}_x\text{-H}_2\text{O-30}$ ; (c)  $\text{Ti}_3\text{C}_2\text{T}_x\text{-NaAsc-0}$ ; (d)  $\text{Ti}_3\text{C}_2\text{T}_x\text{-NaAsc-30}$ .

Ascorbate anions preferred to combine with the edges or defects of  $\text{Ti}_3\text{C}_2\text{T}_x$  by electrostatic interaction, which thus protected  $\text{Ti}_3\text{C}_2\text{T}_x$  from the oxidation. In addition, the dissolved oxygen was considered to be responsible for the poor stability of  $\text{Ti}_3\text{C}_2\text{T}_x$  in aqueous dispersions [44]. As the hydration between Na ions and water prevailed in the competition with that between oxygen and water, there was less dissolved oxygen in  $\text{Ti}_3\text{C}_2\text{T}_x\text{-NaAsc}$  than in  $\text{Ti}_3\text{C}_2\text{T}_x\text{-H}_2\text{O}$  [42]. Therefore,  $\text{Ti}_3\text{C}_2\text{T}_x\text{-NaAsc-30}$  demonstrated much better stability than  $\text{Ti}_3\text{C}_2\text{T}_x\text{-H}_2\text{O-30}$ . TEM images of  $\text{Ti}_3\text{C}_2\text{T}_x\text{-Fresh}$  and  $\text{Ti}_3\text{C}_2\text{T}_x\text{-H}_2\text{O-30}$  were also given in Figure S1. Smooth edges and distinct layered structures can be found in  $\text{Ti}_3\text{C}_2\text{T}_x\text{-Fresh}$ , while they began to blur and even were not observed in  $\text{Ti}_3\text{C}_2\text{T}_x\text{-H}_2\text{O-30}$ , and many small fragments appeared due to oxidation.

To have a better understanding of the morphology change between and after oxidation, SEM images were given for  $\text{Ti}_3\text{C}_2\text{T}_x\text{-Fresh}$ ,  $\text{Ti}_3\text{C}_2\text{T}_x\text{-H}_2\text{O-30}$ , and  $\text{Ti}_3\text{C}_2\text{T}_x\text{-NaAsc-30}$  in Figure 2. The original  $\text{Ti}_3\text{C}_2\text{T}_x\text{-Fresh}$  showed a complete large-size layered structure with a very smooth surface and some clear folds (Figure 2a,b). However,  $\text{Ti}_3\text{C}_2\text{T}_x\text{-H}_2\text{O-30}$  exhibited a fragmented small-size structure with a lot of small white matter on the surface, which may result from  $\text{TiO}_2$  formed at the edge of  $\text{Ti}_3\text{C}_2\text{T}_x$  (Figure 2c,d) [58].  $\text{Ti}_3\text{C}_2\text{T}_x\text{-NaAsc-30}$  still exhibited a large-size layered structure with a smooth surface, and the layered structure was loose; moreover, there was no white matter as was the case in  $\text{Ti}_3\text{C}_2\text{T}_x\text{-H}_2\text{O-30}$ , which meant that the original structure of fresh  $\text{Ti}_3\text{C}_2\text{T}_x$  was kept well in  $\text{Ti}_3\text{C}_2\text{T}_x\text{-NaAsc-30}$  (Figure 2e,f).

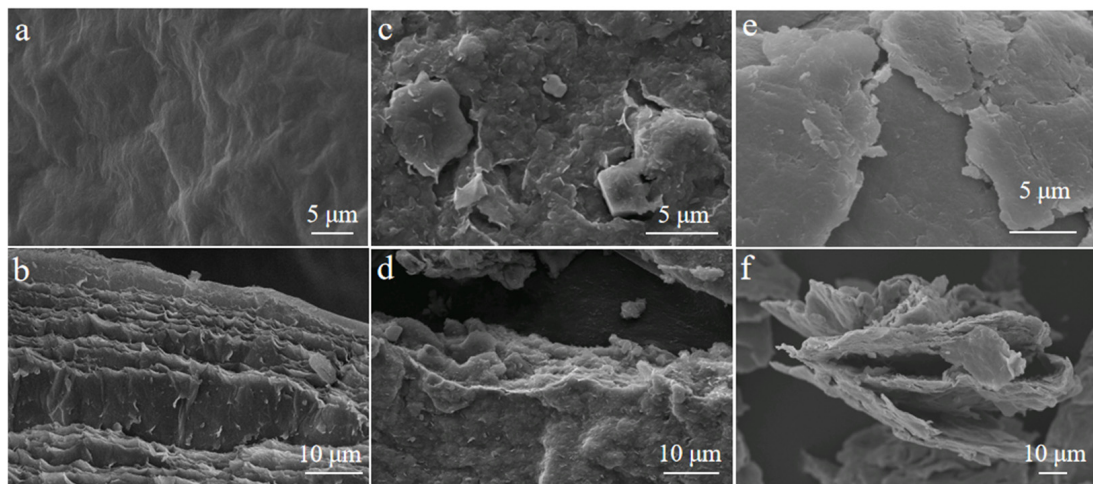


**Figure 2.** SEM images. (a)  $\text{Ti}_3\text{C}_2\text{T}_x$ -Fresh (surface); (b)  $\text{Ti}_3\text{C}_2\text{T}_x$ -Fresh (cross-section); (c)  $\text{Ti}_3\text{C}_2\text{T}_x$ - $\text{H}_2\text{O}$ -30 (surface); (d)  $\text{Ti}_3\text{C}_2\text{T}_x$ - $\text{H}_2\text{O}$ -30 (cross-section); (e)  $\text{Ti}_3\text{C}_2\text{T}_x$ -NaAsc-30 (surface); (f)  $\text{Ti}_3\text{C}_2\text{T}_x$ -NaAsc-30 (cross-section).

Furthermore, the absorption spectra for both  $\text{Ti}_3\text{C}_2\text{T}_x$ - $\text{H}_2\text{O}$  and  $\text{Ti}_3\text{C}_2\text{T}_x$ -NaAsc were investigated as shown in Figure 3, and the evolution of the characteristic absorption of  $\text{Ti}_3\text{C}_2\text{T}_x$  at 773 nm was thus compared [59]. For  $\text{Ti}_3\text{C}_2\text{T}_x$ - $\text{H}_2\text{O}$ , the absorption intensity decreased very fast with the storage time, and it was less than half of the original intensity after 7 days, and there was nearly no absorption feature after 21 days, while  $\text{Ti}_3\text{C}_2\text{T}_x$ -NaAsc exhibited a very stable absorption intensity with the storage time, the absorption intensity gradually became stable after 3 days, and it still kept 75% of the initial intensity even after 21 days. The introduction of NaAsc obviously delayed the reduction of the absorption intensity with the storage time for  $\text{Ti}_3\text{C}_2\text{T}_x$ -NaAsc.

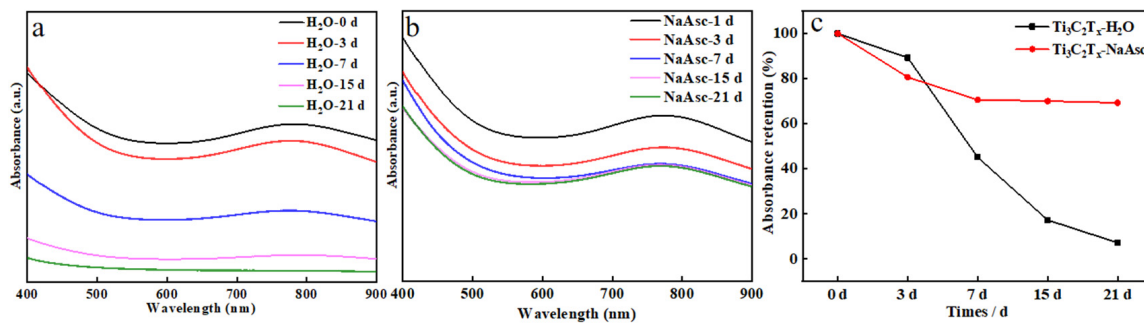


**Figure 3.** UV–vis spectra of MXene with different storage conditions. (a)  $\text{Ti}_3\text{C}_2\text{T}_x$ - $\text{H}_2\text{O}$ ; (b)  $\text{Ti}_3\text{C}_2\text{T}_x$ -NaAsc; (c) change of relative absorption intensity at 773 nm with storage time for  $\text{Ti}_3\text{C}_2\text{T}_x$ - $\text{H}_2\text{O}$  and  $\text{Ti}_3\text{C}_2\text{T}_x$ -NaAsc.

Figure 4 shows the comparison of XRD patterns for  $\text{Ti}_3\text{AlC}_2$ ,  $\text{Ti}_3\text{C}_2\text{T}_x$ -Fresh,  $\text{Ti}_3\text{C}_2\text{T}_x$ - $\text{H}_2\text{O}$ -30, and  $\text{Ti}_3\text{C}_2\text{T}_x$ -NaAsc-30. The (002) peak shifted from a high value in  $\text{Ti}_3\text{AlC}_2$  to a low value in  $\text{Ti}_3\text{C}_2\text{T}_x$ -Fresh, and the typical peak around  $40^\circ$  for Al element disappeared in  $\text{Ti}_3\text{C}_2\text{T}_x$ -Fresh, indicating the successful preparation of  $\text{Ti}_3\text{C}_2\text{T}_x$  with high quality. For  $\text{Ti}_3\text{C}_2\text{T}_x$ -NaAsc-30, the (002) peak showed a slightly lower angle than  $\text{Ti}_3\text{C}_2\text{T}_x$ -Fresh; in addition, its intensity decreased a little bit, resulting from the oxidization of  $\text{Ti}_3\text{C}_2\text{T}_x$  to a certain extent after 30-day storage with NaAsc, and the loose crystal structure was confirmed by SEM in Figure 2f. As a comparison, for  $\text{Ti}_3\text{C}_2\text{T}_x$ - $\text{H}_2\text{O}$ -30, its (002) peak totally disappeared as the layered structure was destroyed during storage, which was consistent with the SEM images in Figure 2c,d.

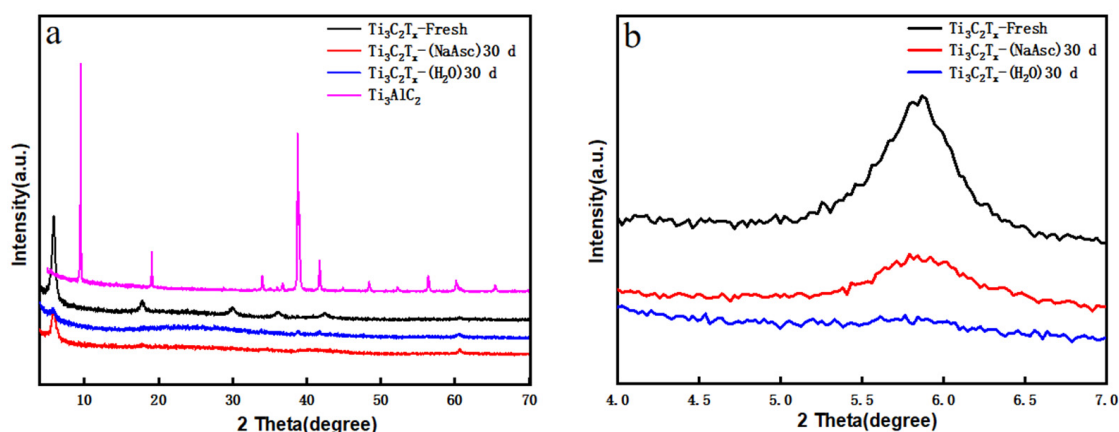


**Figure 4.** XRD patterns for  $\text{Ti}_3\text{C}_2\text{T}_x$  and  $\text{Ti}_3\text{AlC}_2$  in different storage conditions. (a) Full angles and (b) low angles.

According to the Bragg equation

$$2d\sin\theta = n\lambda \quad (2)$$

where  $d$  is the crystal plane spacing,  $\theta$  is the angle between the incident X-ray and the corresponding crystal plane,  $\lambda$  is the wavelength of the X-ray, and  $n$  is the diffraction series,  $\text{Ti}_3\text{C}_2\text{T}_x$ -Fresh and  $\text{Ti}_3\text{C}_2\text{T}_x$ -NaAsc-30 both showed the (002) peak at  $5.86^\circ$ , and the interlayer spacing of  $\text{Ti}_3\text{C}_2\text{T}_x$  nanosheets can be calculated to be 1.52 nm before and after the storage from Equation (2). Combining the SEM and XRD results, the stacking of  $\text{Ti}_3\text{C}_2\text{T}_x$  nanosheets can be well suppressed with the introduction of NaAsc, which is beneficial to ion transport in electrochemical applications.

XPS measurement was conducted on  $\text{Ti}_3\text{C}_2\text{T}_x$ -Fresh,  $\text{Ti}_3\text{C}_2\text{T}_x$ -H<sub>2</sub>O-30, and  $\text{Ti}_3\text{C}_2\text{T}_x$ -NaAsc-30 to understand what happened to  $\text{Ti}_3\text{C}_2\text{T}_x$  in the aqueous dispersion with the storage time (Figure 5). O 1s features were attributed to C-Ti-O (528.0 eV), C-Ti-OH (530.0 eV), and Ti-O (529.2 eV) for  $\text{Ti}_3\text{C}_2\text{T}_x$ -Fresh (Figure 5a). The existence of Ti-O partially resulted from the binding of Ti to surface functional groups (-OH or -O-) of  $\text{Ti}_3\text{C}_2\text{T}_x$ , and also from the oxidization during the preparation of  $\text{Ti}_3\text{C}_2\text{T}_x$ . Ti-O accounted for 15.1% of the oxygen content in  $\text{Ti}_3\text{C}_2\text{T}_x$ -Fresh, while it obviously increased to 70.2% in  $\text{Ti}_3\text{C}_2\text{T}_x$ -H<sub>2</sub>O-30, indicating severe oxidization in a pure aqueous dispersion. The Ti-O content was found to be 31.2% in  $\text{Ti}_3\text{C}_2\text{T}_x$ -NaAsc-30, indicating that the introduction of NaAsc effectively suppressed the oxidization of the MXene. Furthermore, Ti 2p features were divided into Ti-C (453.7 eV), Ti(II) 2p<sub>3/2</sub> (455.3 eV), Ti(III) 2p<sub>3/2</sub> (457.0 eV), and Ti-O 2p<sub>1/2</sub> (463.5 eV) (Figure 5b). Ti-O binding in Ti 2p<sub>1/2</sub> increased significantly in  $\text{Ti}_3\text{C}_2\text{T}_x$ -H<sub>2</sub>O-30, and Ti(III) 2p<sub>3/2</sub> basically shifted to the Ti-O 2p<sub>3/2</sub> binding. In  $\text{Ti}_3\text{C}_2\text{T}_x$ -NaAsc-30, Ti-O 2p<sub>1/2</sub> showed quite similar features with those of  $\text{Ti}_3\text{C}_2\text{T}_x$ -Fresh, which was consistent with the results in O 1s. C 1s showed nearly the same features as  $\text{Ti}_3\text{C}_2\text{T}_x$ -NaAsc-30,  $\text{Ti}_3\text{C}_2\text{T}_x$ -Fresh, and  $\text{Ti}_3\text{C}_2\text{T}_x$ -H<sub>2</sub>O-30 (Figure 5c).

In addition, the conductivity of  $\text{Ti}_3\text{C}_2\text{T}_x$  was measured, which is an important parameter for MXenes, and Table S1 listed the conductivity for  $\text{Ti}_3\text{C}_2\text{T}_x$ -Fresh,  $\text{Ti}_3\text{C}_2\text{T}_x$ -H<sub>2</sub>O, and  $\text{Ti}_3\text{C}_2\text{T}_x$ -NaAsc with the storage time. It was found that the conductivity of  $\text{Ti}_3\text{C}_2\text{T}_x$ -NaAsc stayed at 87.5% in  $\text{Ti}_3\text{C}_2\text{T}_x$ -Fresh after 30 days, while it decreased to less than  $10^{-3} \text{ S m}^{-1}$  in  $\text{Ti}_3\text{C}_2\text{T}_x$ -H<sub>2</sub>O-15. The significant decline in conductivity can also be utilized as a preliminary predictive method for evaluating variations in the stability of MXene dispersions [60].

The stable MXene aqueous dispersion demonstrated potential for the long-term storage of MXenes; moreover, it was quite suitable for the printing process as eco-friendly conductive ink. To understand how the preserved  $\text{Ti}_3\text{C}_2\text{T}_x$  still worked for high-performance supercapacitors, electrochemical measurements were conducted for  $\text{Ti}_3\text{C}_2\text{T}_x$  with different storage conditions. Figure S2 shows the CV curves for  $\text{Ti}_3\text{C}_2\text{T}_x$ -Fresh,  $\text{Ti}_3\text{C}_2\text{T}_x$ -NaAsc-15,

$\text{Ti}_3\text{C}_2\text{T}_x\text{-NaAsc-30}$ , and  $\text{Ti}_3\text{C}_2\text{T}_x\text{-NaAsc-60}$  under different scanning rates, from which all CV curves showed a similar shape with the typical feature of an electric double-layer capacitor (EDLC), and Figure 6a shows the comparison of CV curves for all samples at 5 mV/s.

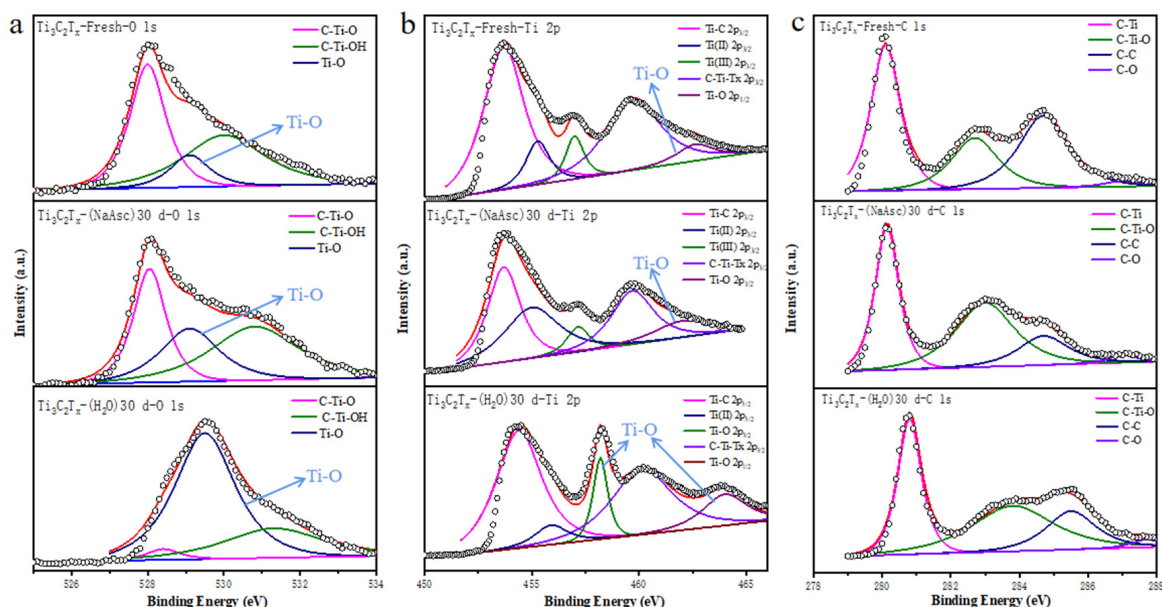


Figure 5. XPS of  $\text{Ti}_3\text{C}_2\text{T}_x\text{-Fresh}$ ,  $\text{Ti}_3\text{C}_2\text{T}_x\text{-H}_2\text{O-30}$ , and  $\text{Ti}_3\text{C}_2\text{T}_x\text{-NaAsc-30}$ . (a) O 1s, (b) Ti 2p, (c) C 1s.

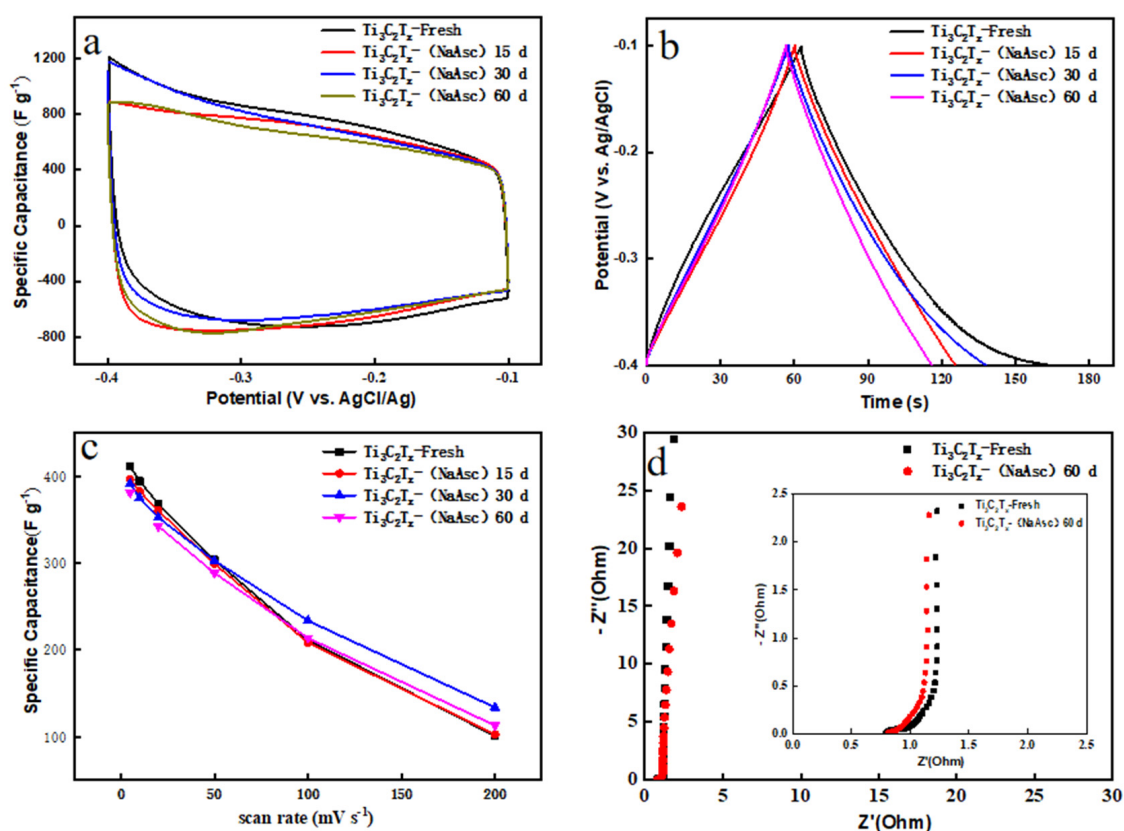


Figure 6. Electrochemical measurements for  $\text{Ti}_3\text{C}_2\text{T}_x$ . (a) CV curves at 5 mV/s; (b) GCD curves at 1 A  $\text{g}^{-1}$ ; (c) specific capacitance with the scanning rate; (d) EIS curves.



Table 1 lists the values of specific capacitance for the different samples. For  $\text{Ti}_3\text{C}_2\text{T}_x$ -Fresh as the electrode, the specific capacitance was 411.4 F/g, and it was 396.3, 391.3, and 381.1 F/g for  $\text{Ti}_3\text{C}_2\text{T}_x$ -NaAsc-15,  $\text{Ti}_3\text{C}_2\text{T}_x$ -NaAsc-30, and  $\text{Ti}_3\text{C}_2\text{T}_x$ -NaAsc-60, respectively. Compared with the fresh  $\text{Ti}_3\text{C}_2\text{T}_x$ , the specific capacitance kept 96.3%, 95.1%, and 92.6% of the original value after the storage of 15, 30, and 60 days, respectively. Even at a high scanning rate of 200 mV/s,  $\text{Ti}_3\text{C}_2\text{T}_x$ -NaAsc still showed a large specific capacitance. For example, after 60-day storage,  $\text{Ti}_3\text{C}_2\text{T}_x$ -NaAsc-60 demonstrated 112.8 F/g, which was even higher than  $\text{Ti}_3\text{C}_2\text{T}_x$ -Fresh at the same scanning rate. Figure S3 shows the GCD curves for  $\text{Ti}_3\text{C}_2\text{T}_x$ -Fresh,  $\text{Ti}_3\text{C}_2\text{T}_x$ -NaAsc-15,  $\text{Ti}_3\text{C}_2\text{T}_x$ -NaAsc-30, and  $\text{Ti}_3\text{C}_2\text{T}_x$ -NaAsc-60 at different current densities. They all demonstrated similar and symmetric triangular curves, indicating good capacitance characteristics and reversibility, and the preserved  $\text{Ti}_3\text{C}_2\text{T}_x$  exhibited almost the same GCD behavior as the fresh  $\text{Ti}_3\text{C}_2\text{T}_x$  (Figure 6b). Furthermore, the cyclic stability was characterized at 50 mV/s (Figure S4), and after 10,000 CV cycles, the specific capacitance was maintained at 99.4%, 99.6%, 99.0%, and 99.5% for  $\text{Ti}_3\text{C}_2\text{T}_x$ -Fresh,  $\text{Ti}_3\text{C}_2\text{T}_x$ -NaAsc-15,  $\text{Ti}_3\text{C}_2\text{T}_x$ -NaAsc-30, and  $\text{Ti}_3\text{C}_2\text{T}_x$ -NaAsc-60, respectively. Figure 6c shows the evolution of specific capacitance with the scanning rate. A slightly reduced specific capacitance was observed for  $\text{Ti}_3\text{C}_2\text{T}_x$  after the storage with NaAsc, which may be due to the unsaturation of NaAsc in the aqueous solution. Therefore, the defects of  $\text{Ti}_3\text{C}_2\text{T}_x$  were not totally combined with ascorbate anions. Related studies indicated that the best antioxidant effect on MXenes is obtained when the salt solution reaches saturation [42]. Figure 6d shows the comparison of EIS curves for  $\text{Ti}_3\text{C}_2\text{T}_x$ -Fresh and  $\text{Ti}_3\text{C}_2\text{T}_x$ -NaAsc-60, which exhibit quite similar EIS curves, indicating that  $\text{Ti}_3\text{C}_2\text{T}_x$  can be kept well in an aqueous dispersion long term with the introduction of NaAsc. Figure S5 and Table S2 show the comparison of electrochemical properties for  $\text{Ti}_3\text{C}_2\text{T}_x$ -fresh and  $\text{Ti}_3\text{C}_2\text{T}_x$ -H<sub>2</sub>O-30, indicating bad performance without the introduction of NaAsc.

**Table 1.** Specific capacitance (F/g) of  $\text{Ti}_3\text{C}_2\text{T}_x$  at 1M H<sub>2</sub>SO<sub>4</sub> electrolyte.

	5 mV/s	10 mV/s	20 mV/s	50 mV/s	100 mV/s	200 mV/s
<b><math>\text{Ti}_3\text{C}_2\text{T}_x</math>-Fresh</b>	411.4	394.2	368.5	303.5	211.1	100.7
<b><math>\text{Ti}_3\text{C}_2\text{T}_x</math>-NaAsc-15</b>	396.3	382.7	360.5	299.2	208.2	102.5
<b><math>\text{Ti}_3\text{C}_2\text{T}_x</math>-NaAsc-30</b>	391.3	374.7	352.4	302.6	233.4	133.6
<b><math>\text{Ti}_3\text{C}_2\text{T}_x</math>-NaAsc-60</b>	381.1	364.7	342.5	288.5	213.5	112.8

The effect of the antioxidant is to protect the edges and defects of  $\text{Ti}_3\text{C}_2\text{T}_x$  from water and oxygen [58]. When an antioxidant was used, such as an anionic surfactant SDS [61], Tris-HCl [62], or NaAsc [58], they preferred to interact with positively charged groups on the  $\text{Ti}_3\text{C}_2\text{T}_x$  surface, which obstructed the interaction between water/oxygen molecules and Ti/C constituents within the  $\text{Ti}_3\text{C}_2\text{T}_x$ ; thus, the stability of  $\text{Ti}_3\text{C}_2\text{T}_x$  was greatly improved, and its electrochemical performance can be well kept. Here, the NaAsc-treated dispersion maintained colloidal stability even after 60 days at room temperature, with the 2D layered structure preserved as evidenced by SEM, and the stored  $\text{Ti}_3\text{C}_2\text{T}_x$  exhibited the specific capacitance of 381.1 F/g after 10,000 cycles with a capacitance retention of 92.6%, which was comparable to that of the fresh  $\text{Ti}_3\text{C}_2\text{T}_x$ . Although  $\text{Ti}_3\text{C}_2\text{T}_x$  treated with hyperbranched polyethylene ionomers can be stably preserved in both aqueous and organic phases for a duration of 100 days, the data are absent regarding the electrochemical performance of long-term storage [63]. In addition, the functionalization of  $\text{Ti}_3\text{C}_2\text{T}_x$ , such as with an amino-functionalized MXene, is a feasible way to improve its electrochemical performance through surface modification. Moreover, the stability of  $\text{Ti}_3\text{C}_2\text{T}_x$  can be enhanced as well [64]. Table 2 compares the electrochemical performance of the  $\text{Ti}_3\text{C}_2\text{T}_x$  aqueous dispersion with different antioxidant methods.

**Table 2.** Electrochemical performance of  $\text{Ti}_3\text{C}_2\text{T}_x$  with different antioxidant methods.

Antioxidant	Time (Day)	Electrolyte	Rate (mV/s)	Capacitance (F/g)	Retention	Ref
SDS	35	3 M $\text{H}_2\text{SO}_4$	-	~300 <sup>a</sup>	95.4%	[61]
Tris-HCl	35	3 M $\text{H}_2\text{SO}_4$	-	251.6 <sup>a</sup>	94.6%	[62]
HPI	-	$[\text{EMIM}]^+$ $[\text{BF}_4]^-$	2	220 <sup>b</sup>	-	[63]
NaAsc	60	1 M $\text{H}_2\text{SO}_4$	5	381.1 <sup>b</sup>	92.6%	Here

All experimental conditions were maintained at room temperature, with a and b representing the calculations of specific capacitance derived from GCD and CV methods, respectively.

#### 4. Conclusions

In summary, we investigated the effect of NaAsc on the long-term storage of  $\text{Ti}_3\text{C}_2\text{T}_x$ , emphasizing its electrochemical performance across various storage stages. The findings demonstrated that NaAsc significantly enhanced the stability of  $\text{Ti}_3\text{C}_2\text{T}_x$  in aqueous dispersions, with ascorbic ions interacting with the cationic groups on the MXene surface, effectively protecting it from water and oxygen. Remarkably, even after 60 days of storage, its layered structure, dispersibility, and electrochemical properties remained largely intact. To assess electrochemical performance, the specific capacitance of supercapacitors utilizing MXenes as electrodes reached 381.1 F/g at a scan rate of 5 mV/s, with a capacitance retention rate of 92.6% after 10,000 CV cycles, comparable to that of fresh MXenes. Thus, our findings propose an effective approach for the long-term storage of MXenes with minimal attenuation of their electrochemical performance, which shows great potential for large-scale application of MXenes in energy storage.

**Supplementary Materials:** The following supporting information can be downloaded at: <https://www.mdpi.com/article/10.3390/ma17225414/s1>, Figure S1: TEM images. (a)  $\text{Ti}_3\text{C}_2\text{T}_x$ -Fresh; (b)  $\text{Ti}_3\text{C}_2\text{T}_x$ - $\text{H}_2\text{O}$ -30. Figure S2: CV curves. (a)  $\text{Ti}_3\text{C}_2\text{T}_x$ -Fresh; (b)  $\text{Ti}_3\text{C}_2\text{T}_x$ -NaAsc-15; (c)  $\text{Ti}_3\text{C}_2\text{T}_x$ -NaAsc-30; (d)  $\text{Ti}_3\text{C}_2\text{T}_x$ -NaAsc-60. Figure S3: GCD curves. (a)  $\text{Ti}_3\text{C}_2\text{T}_x$ -Fresh; (b)  $\text{Ti}_3\text{C}_2\text{T}_x$ -NaAsc-15; (c)  $\text{Ti}_3\text{C}_2\text{T}_x$ -NaAsc-30; (d)  $\text{Ti}_3\text{C}_2\text{T}_x$ -NaAsc-60. Figure S4: Cyclic stability at 50 mV s<sup>-1</sup>. (a)  $\text{Ti}_3\text{C}_2\text{T}_x$ -Fresh; (b)  $\text{Ti}_3\text{C}_2\text{T}_x$ -NaAsc-15; (c)  $\text{Ti}_3\text{C}_2\text{T}_x$ -NaAsc-30; (d)  $\text{Ti}_3\text{C}_2\text{T}_x$ -NaAsc-60. The inserted indicates the comparison of CV curves between cycle 1 and cycle 10,000. Figure S5: Electrochemical measurements for  $\text{Ti}_3\text{C}_2\text{T}_x$ -fresh and  $\text{Ti}_3\text{C}_2\text{T}_x$ - $\text{H}_2\text{O}$ -30. (a) CV curves at 5 mV/s; (b) GCD curves at 1 A g<sup>-1</sup>. Table S1. Conductivity (S m<sup>-1</sup>) of various filtration membranes. Table S2. Specific capacitance (F g<sup>-1</sup>) of  $\text{Ti}_3\text{C}_2\text{T}_x$ -fresh and  $\text{Ti}_3\text{C}_2\text{T}_x$ - $\text{H}_2\text{O}$ -30.

**Author Contributions:** Methodology, T.P. and R.W.; Software, B.W.; Validation, R.W. and B.W.; Formal analysis, T.P.; Investigation, T.P. and T.L.; Resources, B.W.; Data curation, R.W.; Writing—original draft, T.P.; Writing—review & editing, T.L. and S.S.; Supervision, S.S.; Project administration, S.S.; Funding acquisition, S.S. All authors have read and agreed to the published version of the manuscript.

**Funding:** This project was financially supported by the National Natural Science Foundation of China (52173183) and the opening project of the Key Laboratory of Optoelectronic Chemical Materials and Devices of Ministry of Education (Jiangnan University) (JDGD-202207).

**Institutional Review Board Statement:** Not applicable.

**Informed Consent Statement:** Not applicable.

**Data Availability Statement:** The original contributions presented in the study are included in the article/Supplementary Materials, further inquiries can be directed to the corresponding authors.

**Conflicts of Interest:** The authors declare no conflict of interest.

#### References

- Naguib, M.; Mochalin, V.N.; Barsoum, M.W.; Gogotsi, Y. 25th Anniversary Article: MXenes: A New Family of Two-Dimensional Materials. *Adv. Mater.* **2014**, *26*, 992–1005. [[CrossRef](#)] [[PubMed](#)]
- Li, X.; Huang, Z.; Shuck, C.E.; Liang, G.; Gogotsi, Y.; Zhi, C. MXene Chemistry, Electrochemistry and Energy Storage Applications. *Nat. Rev. Chem.* **2022**, *6*, 389–404. [[CrossRef](#)] [[PubMed](#)]

3. Xu, J.; Peng, T.; Qin, X.; Zhang, Q.; Liu, T.; Dai, W.; Chen, B.; Yu, H.; Shi, S. Recent Advances in 2D MXenes: Preparation, Intercalation and Applications in Flexible Devices. *J. Mater. Chem. A* **2021**, *9*, 14147–14171. [[CrossRef](#)]
4. Naguib, M.; Kurtoglu, M.; Presser, V.; Lu, J.; Niu, J.; Heon, M.; Hultman, L.; Gogotsi, Y.; Barsoum, M.W. Two-Dimensional Nanocrystals Produced by Exfoliation of  $Ti_3AlC_2$ . *Adv. Mater.* **2011**, *23*, 4248–4253. [[CrossRef](#)] [[PubMed](#)]
5. Ghidoui, M.; Lukatskaya, M.R.; Zhao, M.Q.; Gogotsi, Y.; Barsoum, M.W. Conductive Two-Dimensional Titanium Carbide “clay” with High Volumetric Capacitance. *Nature* **2015**, *516*, 78–81. [[CrossRef](#)]
6. Li, T.; Yao, L.; Liu, Q.; Gu, J.; Luo, R.; Li, J.; Yan, X.; Wang, W.; Liu, P.; Chen, B.; et al. Fluorine-Free Synthesis of High-Purity  $Ti_3C_2T_x$  ( $T=OH, O$ ) via Alkali Treatment. *Angew. Chem.-Int. Ed.* **2018**, *57*, 6115–6119. [[CrossRef](#)]
7. Hart, J.L.; Hantanasirisakul, K.; Lang, A.C.; Anasori, B.; Pinto, D.; Pivak, Y.; van Omme, J.T.; May, S.J.; Gogotsi, Y.; Taheri, M.L. Control of MXenes’ Electronic Properties through Termination and Intercalation. *Nat. Commun.* **2019**, *10*, 522. [[CrossRef](#)]
8. Zhang, Y.Z.; Lee, K.H.; Anjum, D.H.; Sougrat, R.; Jiang, Q.; Kim, H.; Alshareef, H.N. MXenes Stretch Hydrogel Sensor Performance to New Limits. *Sci. Adv.* **2018**, *4*, eaat0098. [[CrossRef](#)]
9. Ma, Y.; Liu, N.; Li, L.; Hu, X.; Zou, Z.; Wang, J.; Luo, S.; Gao, Y. A Highly Flexible and Sensitive Piezoresistive Sensor Based on MXene with Greatly Changed Interlayer Distances. *Nat. Commun.* **2017**, *8*, 1207. [[CrossRef](#)]
10. Lu, Y.; Qu, X.; Zhao, W.; Ren, Y.; Si, W.; Wang, W.; Wang, Q.; Huang, W.; Dong, X. Highly Stretchable, Elastic, and Sensitive MXene-Based Hydrogel for Flexible Strain and Pressure Sensors. *Research* **2020**, *2020*, 2038560. [[CrossRef](#)]
11. Gao, L.; Wang, M.; Wang, W.; Xu, H.; Wang, Y.; Zhao, H.; Cao, K.; Xu, D.; Li, L. Highly Sensitive Pseudocapacitive Iontronic Pressure Sensor with Broad Sensing Range. *Nano-Micro Lett.* **2021**, *13*, 140. [[CrossRef](#)] [[PubMed](#)]
12. Choi, J.; Chacon, B.; Park, H.; Hantanasirisakul, K.; Kim, T.; Shevchuk, K.; Lee, J.; Kang, H.; Cho, S.Y.; Kim, J.; et al. N-p-Conductor Transition of Gas Sensing Behaviors in  $Mo_2CT_x$  MXene. *ACS Sens.* **2022**, *7*, 2225–2234. [[CrossRef](#)] [[PubMed](#)]
13. Zhang, F.; Yang, L.; Yan, H.; Tian, B.; Zhu, X. Black Graphitic Carbon Nitride Nanosheets with Mid-Gap States Realizing Highly Efficient Near-Infrared Photo-Thermal Conversion for Photoacoustic Imaging. *J. Mater. Chem. B* **2022**, *47*, 9923–9930. [[CrossRef](#)]
14. Ma, R.; Chen, Z.; Zhao, D.; Zhang, X.; Zhuo, J.; Yin, Y.; Wang, X.; Yang, G.; Yi, F.  $Ti_3C_2T_x$ : MXene for Electrode Materials of Supercapacitors. *J. Mater. Chem. A* **2021**, *9*, 11501–11529. [[CrossRef](#)]
15. Simon, P.; Gogotsi, Y. Perspectives for Electrochemical Capacitors and Related Devices. *Nat. Mater.* **2020**, *19*, 1151–1163. [[CrossRef](#)] [[PubMed](#)]
16. Zhang, P.; Li, J.; Yang, D.; Soomro, R.A.; Xu, B. Flexible Carbon Dots-Intercalated MXene Film Electrode with Outstanding Volumetric Performance for Supercapacitors. *Adv. Funct. Mater.* **2023**, *33*, 2209918. [[CrossRef](#)]
17. Feng, S.; Wang, X.; Wang, M.; Bai, C.; Cao, S.; Kong, D. Crumpled MXene Electrodes for Ultrastretchable and High-Area-Capacitance Supercapacitors. *Nano Lett.* **2021**, *21*, 7561–7568. [[CrossRef](#)]
18. Xu, J.; Peng, T.; Zhang, Q.; Zheng, H.; Yu, H.; Shi, S. Intercalation Effects on the Electrochemical Properties of  $Ti_3C_2T_x$  MXene Nanosheets for High-Performance Supercapacitors. *ACS Appl. Nano Mater.* **2022**, *5*, 8794–8803. [[CrossRef](#)]
19. Yu, Z.; Feng, W.; Lu, W.; Li, B.; Yao, H.; Zeng, K.; Ouyang, J. MXenes with Tunable Work Functions and Their Application as Electron- and Hole-Transport Materials in Non-Fullerene Organic Solar Cells. *J. Mater. Chem. A* **2019**, *7*, 11160–11169. [[CrossRef](#)]
20. Sun, B.; Lu, Q.; Chen, K.; Zheng, W.; Liao, Z.; Lopatik, N.; Li, D.; Hantusch, M.; Zhou, S.; Wang, H.I.; et al. Redox-Active Metaphosphate-Like Terminals Enable High-Capacity MXene Anodes for Ultrafast Na-Ion Storage. *Adv. Mater.* **2022**, *34*, 2108682. [[CrossRef](#)]
21. Wang, X.; Luo, D.; Wang, J.; Sun, Z.; Cui, G.; Chen, Y.; Wang, T.; Zheng, L.; Zhao, Y.; Shui, L.; et al. Strain Engineering of a MXene/CNT Hierarchical Porous Hollow Microsphere Electrocatalyst for a High-Efficiency Lithium Polysulfide Conversion Process. *Angew. Chem.-Int. Ed.* **2021**, *60*, 2371–2378. [[CrossRef](#)] [[PubMed](#)]
22. Dong, Y.; Shi, H.; Wu, Z.S. Recent Advances and Promise of MXene-Based Nanostructures for High-Performance Metal Ion Batteries. *Adv. Funct. Mater.* **2020**, *30*, 2000706. [[CrossRef](#)]
23. Mashtalir, O.; Cook, K.M.; Mochalin, V.N.; Crowe, M.; Barsoum, M.W.; Gogotsi, Y. Dye Adsorption and Decomposition on Two-Dimensional Titanium Carbide in Aqueous Media. *J. Mater. Chem. A* **2014**, *2*, 14334–14338. [[CrossRef](#)]
24. Seh, Z.W.; Fredrickson, K.D.; Anasori, B.; Kibsgaard, J.; Strickler, A.L.; Lukatskaya, M.R.; Gogotsi, Y.; Jaramillo, T.F.; Vojvodic, A. Two-Dimensional Molybdenum Carbide (MXene) as an Efficient Electrocatalyst for Hydrogen Evolution. *ACS Energy Lett.* **2016**, *1*, 589–594. [[CrossRef](#)]
25. Yu, Y.; Zhou, J.; Sun, Z. Novel 2D Transition-Metal Carbides: Ultrahigh Performance Electrocatalysts for Overall Water Splitting and Oxygen Reduction. *Adv. Funct. Mater.* **2020**, *30*, 2000570. [[CrossRef](#)]
26. Morales-García, Á.; Calle-Vallejo, F.; Illas, F. MXenes: New Horizons in Catalysis. *ACS Catal.* **2020**, *10*, 13487–13503. [[CrossRef](#)]
27. Iqbal, A.; Shahzad, F.; Hantanasirisakul, K.; Kim, M.K.; Kwon, J.; Hong, J.; Kim, H.; Kim, D.; Gogotsi, Y.; Koo, C.M. Anomalous Absorption of Electromagnetic Waves by 2D Transition Metal Carbonitride  $Ti_3CNT_x$  (MXene). *Science* **2020**, *369*, 446–450. [[CrossRef](#)]
28. Shahzad, F.; Alhabeb, M.; Hatter, C.B.; Anasori, B.; Hong, S.M.; Koo, C.M.; Gogotsi, Y. Electromagnetic Interference Shielding with 2D Transition Metal Carbides (MXenes). *Science* **2016**, *353*, 1137–1140. [[CrossRef](#)]
29. Liu, J.; Zhang, H.B.; Sun, R.; Liu, Y.; Liu, Z.; Zhou, A.; Yu, Z.Z. Hydrophobic, Flexible, and Lightweight MXene Foams for High-Performance Electromagnetic-Interference Shielding. *Adv. Mater.* **2017**, *29*, 1702367. [[CrossRef](#)]

30. Chen, W.; Liu, L.-X.; Zhang, H.-B.; Yu, Z.-Z. Flexible, Transparent, and Conductive Ti<sub>3</sub>C<sub>2</sub>T<sub>x</sub> MXene-Silver Nanowire Films with Smart Acoustic Sensitivity for High-Performance Electromagnetic Interference Shielding. *ACS Nano* **2020**, *14*, 16643–16653. [[CrossRef](#)]
31. Han, M.; Shuck, C.E.; Singh, A.; Yang, Y.; Foucher, A.C.; Goad, A.; McBride, B.; May, S.J.; Shenoy, V.B.; Stach, E.A.; et al. Efficient Microwave Absorption with V<sub>n+1</sub>C<sub>n</sub>T<sub>x</sub> MXenes. *Cell Rep. Phys. Sci.* **2022**, *3*, 101073. [[CrossRef](#)]
32. Zhang, H.; Wan, J.; Wu, R.; Chen, Y.; Yu, H.; Shi, S. MXenes for Electromagnetic Interference Shielding: Insights from Structural Design. *Carbon* **2024**, *218*, 118716. [[CrossRef](#)]
33. Hou, C.; Huang, C.; Yu, H.; Shi, S. Surface-Engineered Ti<sub>3</sub>C<sub>2</sub>T<sub>x</sub> with Tunable Work Functions for Highly Efficient Polymer Solar Cells. *Small* **2022**, *18*, 2201046. [[CrossRef](#)]
34. Huang, C.; Shi, S.; Yu, H. Work Function Adjustment of Nb<sub>2</sub>CT<sub>x</sub> Nanoflakes as Hole and Electron Transport Layers in Organic Solar Cells by Controlling Surface Functional Groups. *ACS Energy Lett.* **2021**, *6*, 3464–3472. [[CrossRef](#)]
35. Zhang, J.; Huang, C.; Sun, Y.; Yu, H. Amino-Functionalized Niobium-Carbide MXene Serving as Electron Transport Layer and Perovskite Additive for the Preparation of High-Performance and Stable Methylammonium-Free Perovskite Solar Cells. *Adv. Funct. Mater.* **2022**, *32*, 2113367. [[CrossRef](#)]
36. Zhou, H.; Han, S.J.; Lee, H.; Zhang, D.; Anayee, M.; Jo, S.H.; Gogotsi, Y.; Lee, T. Overcoming the Limitations of MXene Electrodes for Solution-Processed Optoelectronic Devices. *Adv. Mater.* **2022**, *34*, 2206377. [[CrossRef](#)]
37. Ahn, S.; Han, T.H.; Maleski, K.; Song, J.; Kim, Y.H.; Park, M.H.; Zhou, H.; Yoo, S.; Gogotsi, Y.; Lee, T.W. A 2D Titanium Carbide MXene Flexible Electrode for High-Efficiency Light-Emitting Diodes. *Adv. Mater.* **2020**, *32*, 2000919. [[CrossRef](#)]
38. Driscoll, N.; Erickson, B.; Murphy, B.B.; Richardson, A.G.; Robbins, G.; Apollo, N.V.; Mentzelopoulos, G.; Mathis, T.; Hantanasirisakul, K.; Bagga, P.; et al. MXene-Infused Bioelectronic Interfaces for Multiscale Electrophysiology and Stimulation. *Sci. Transl. Med.* **2021**, *13*, eabf8629. [[CrossRef](#)]
39. Xu, D.; Li, Z.; Li, L.; Wang, J. Insights into the Photothermal Conversion of 2D MXene Nanomaterials: Synthesis, Mechanism, and Applications. *Adv. Funct. Mater.* **2020**, *30*, 2000712. [[CrossRef](#)]
40. Hazan, A.; Ratzker, B.; Zhang, D.; Katiyi, A.; Sokol, M.; Gogotsi, Y.; Karabchevsky, A. MXene-Nanoflakes-Enabled All-Optical Nonlinear Activation Function for On-Chip Photonic Deep Neural Networks. *Adv. Mater.* **2023**, *35*, 2210216. [[CrossRef](#)]
41. Sokolov, A.; Ali, M.; Li, H.; Jeon, Y.R.; Ko, M.J.; Choi, C. Partially Oxidized MXene Ti<sub>3</sub>C<sub>2</sub>T<sub>x</sub> Sheets for Memristor Having Synapse and Threshold Resistive Switching Characteristics. *Adv. Electron. Mater.* **2021**, *7*, 2000866. [[CrossRef](#)]
42. Wang, X.; Wang, Z.; Qiu, J. Stabilizing MXene by Hydration Chemistry in Aqueous Solution. *Angew. Chem.-Int. Ed.* **2021**, *60*, 26587–26591. [[CrossRef](#)] [[PubMed](#)]
43. Cao, F.; Zhang, Y.; Wang, H.; Khan, K.; Tareen, A.K.; Qian, W.; Zhang, H.; Ågren, H. Recent Advances in Oxidation Stable Chemistry of 2D MXenes. *Adv. Mater.* **2022**, *34*, 2107554. [[CrossRef](#)]
44. Huang, S.; Mochalin, V.N. Hydrolysis of 2D Transition-Metal Carbides (MXenes) in Colloidal Solutions. *Inorg. Chem.* **2019**, *58*, 1958–1966. [[CrossRef](#)] [[PubMed](#)]
45. Shuck, C.E.; Han, M.; Maleski, K.; Hantanasirisakul, K.; Kim, S.J.; Choi, J.; Reil, W.E.B.; Gogotsi, Y. Effect of Ti<sub>3</sub>AlC<sub>2</sub> MAX Phase on Structure and Properties of Resultant Ti<sub>3</sub>C<sub>2</sub>T<sub>x</sub> MXene. *ACS Appl. Nano Mater.* **2019**, *2*, 3368–3376. [[CrossRef](#)]
46. Mathis, T.S.; Maleski, K.; Goad, A.; Sarycheva, A.; Anayee, M.; Foucher, A.C.; Hantanasirisakul, K.; Shuck, C.E.; Stach, E.A.; Gogotsi, Y. Modified MAX Phase Synthesis for Environmentally Stable and Highly Conductive Ti<sub>3</sub>C<sub>2</sub> MXene. *ACS Nano* **2021**, *15*, 6420–6429. [[CrossRef](#)]
47. Zhang, C.J.; Pinilla, S.; McEvoy, N.; Cullen, C.P.; Anasori, B.; Long, E.; Park, S.H.; Seral-Ascaso, A.; Shmeliov, A.; Krishnan, D.; et al. Oxidation Stability of Colloidal Two-Dimensional Titanium Carbides (MXenes). *Chem. Mater.* **2017**, *29*, 4848–4856. [[CrossRef](#)]
48. Zhang, J.; Kong, N.; Hegh, D.; Usman, K.A.S.; Guan, G.; Qin, S.; Jurewicz, I.; Yang, W.; Razal, J.M. Freezing Titanium Carbide Aqueous Dispersions for Ultra-Long-Term Storage. *ACS Appl. Mater. Interfaces* **2020**, *12*, 34032–34040. [[CrossRef](#)] [[PubMed](#)]
49. Chae, Y.; Kim, S.J.; Cho, S.Y.; Choi, J.; Maleski, K.; Lee, B.J.; Jung, H.T.; Gogotsi, Y.; Lee, Y.; Ahn, C.W. An Investigation into the Factors Governing the Oxidation of Two-Dimensional Ti<sub>3</sub>C<sub>2</sub> MXene. *Nanoscale* **2019**, *11*, 8387–8393. [[CrossRef](#)]
50. Zhang, Q.; Lai, H.; Fan, R.; Ji, P.; Fu, X.; Li, H. High Concentration of Ti<sub>3</sub>C<sub>2</sub>T<sub>x</sub> MXene in Organic Solvent. *ACS Nano* **2021**, *15*, 5249–5262. [[CrossRef](#)]
51. Maleski, K.; Mochalin, V.N.; Gogotsi, Y. Dispersions of Two-Dimensional Titanium Carbide MXene in Organic Solvents. *Chem. Mater.* **2017**, *29*, 1632–1640. [[CrossRef](#)]
52. Seyedin, S.; Zhang, J.; Usman, K.A.S.; Qin, S.; Glushenkov, A.M.; Yanza, E.R.S.; Jones, R.T.; Razal, J.M. Facile Solution Processing of Stable MXene Dispersions towards Conductive Composite Fibers. *Glob. Chall.* **2019**, *3*, 1900037. [[CrossRef](#)]
53. Kim, J.; Yoon, Y.; Kim, S.K.; Park, S.; Song, W.; Myung, S.; Jung, H.K.; Lee, S.S.; Yoon, D.H.; An, K.S. Chemically Stabilized and Functionalized 2D-MXene with Deep Eutectic Solvents as Versatile Dispersion Medium. *Adv. Funct. Mater.* **2021**, *31*, 2008722. [[CrossRef](#)]
54. Lee, Y.; Kim, S.J.; Kim, Y.J.; Lim, Y.; Chae, Y.; Lee, B.J.; Kim, Y.T.; Han, H.; Gogotsi, Y.; Ahn, C.W. Oxidation-Resistant Titanium Carbide MXene Films. *J. Mater. Chem. A* **2020**, *8*, 573–581. [[CrossRef](#)]
55. Zhao, X.; Holta, D.E.; Tan, Z.; Oh, J.H.; Echols, I.J.; Anas, M.; Cao, H.; Lutkenhaus, J.L.; Radovic, M.; Green, M.J. Annealed Ti<sub>3</sub>C<sub>2</sub>T<sub>x</sub> MXene Films for Oxidation-Resistant Functional Coatings. *ACS Appl. Nano Mater.* **2020**, *3*, 10578–10585. [[CrossRef](#)]

56. Natu, V.; Hart, J.L.; Sokol, M.; Chiang, H.; Taheri, M.L.; Barsoum, M.W. Edge Capping of 2D-MXene Sheets with Polyanionic Salts To Mitigate Oxidation in Aqueous Colloidal Suspensions. *Angew. Chem.-Int. Ed.* **2019**, *58*, 12655–12660. [[CrossRef](#)] [[PubMed](#)]
57. Zhao, X.; Vashisth, A.; Blivin, J.W.; Tan, Z.; Holta, D.E.; Kotasthane, V.; Shah, S.A.; Habib, T.; Liu, S.; Lutkenhaus, J.L.; et al. PH, Nanosheet Concentration, and Antioxidant Affect the Oxidation of  $Ti_3C_2T_x$  and  $Ti_2CT_x$  MXene Dispersions. *Adv. Mater. Interfaces* **2020**, *7*, 2000845. [[CrossRef](#)]
58. Zhao, X.; Vashisth, A.; Prehn, E.; Sun, W.; Shah, S.A.; Habib, T.; Chen, Y.; Tan, Z.; Lutkenhaus, J.L.; Radovic, M.; et al. Antioxidants Unlock Shelf-Stable  $Ti_3C_2T_x$  (MXene) Nanosheet Dispersions. *Matter* **2019**, *1*, 513–526. [[CrossRef](#)]
59. Doo, S.; Chae, A.; Kim, D.; Oh, T.; Ko, T.Y.; Kim, S.J.; Koh, D.Y.; Koo, C.M. Mechanism and Kinetics of Oxidation Reaction of Aqueous  $Ti_3C_2T_x$  Suspensions at Different PHs and Temperatures. *ACS Appl. Mater. Interfaces* **2021**, *13*, 22855–22865. [[CrossRef](#)]
60. Habib, T.; Zhao, X.; Shah, S.A.; Chen, Y.; Sun, W.; An, H.; Lutkenhaus, J.L.; Radovic, M.; Green, M.J. Oxidation Stability of  $Ti_3C_2T_x$  MXene Nanosheets in Solvents and Composite Films. *NPJ 2D Mater. Appl.* **2019**, *3*, 8. [[CrossRef](#)]
61. Fan, B.; Zhao, X.; Zhang, P.; Wei, Y.; Qiao, N.; Yang, B.; Soomro, R.A.; Zhang, R.; Xu, B. Effect of Sodium Dodecyl Sulfate on Stability of MXene Aqueous Dispersion. *Adv. Sci.* **2023**, *10*, 2300273. [[CrossRef](#)] [[PubMed](#)]
62. Tan, J.; Fan, B.; Zhang, P.; Wei, Y.; Soomro, R.A.; Zhao, X.; Kumar, J. Ultralong Stability of  $Ti_3C_2T_x$  MXene Dispersion Through Synergistic Regulation of Storage Environment and Defect Capping with Tris-HCl Buffering. *Small Methods* **2024**, *8*, 2301689. [[CrossRef](#)] [[PubMed](#)]
63. Raisi, B.; Huang, L.; Ye, Z. Modification of  $Ti_3C_2T_x$  MXene with Hyperbranched Polyethylene Ionomers: Stable Dispersions in Nonpolar/Low-Polarity Organic Solvents, Oxidation Protection, and Potential Application in Supercapacitors. *J. Mater. Chem. A* **2023**, *11*, 17167–17187. [[CrossRef](#)]
64. Wan, J.; Wu, R.; Chen, Y.; Zhang, H.; Li, H.; Wang, B.; Liskiewicz, T.; Shi, S. Amino Modification of  $Ti_3C_2$  MXenes for High-Performance Supercapacitors. *Appl. Surf. Sci.* **2024**, *678*, 161154. [[CrossRef](#)]

**Disclaimer/Publisher's Note:** The statements, opinions and data contained in all publications are solely those of the individual author(s) and contributor(s) and not of MDPI and/or the editor(s). MDPI and/or the editor(s) disclaim responsibility for any injury to people or property resulting from any ideas, methods, instructions or products referred to in the content.